Article

One Earth

Global mercury emissions from wildfires are three times lower than existing estimates

Graphical abstract

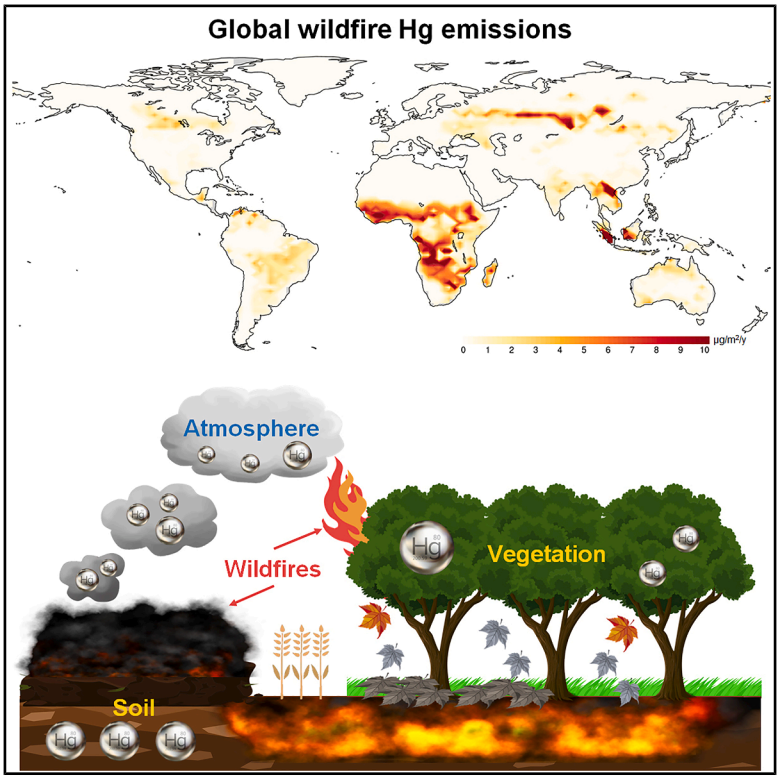

Highlights

- Coupled model reveals that wildfire mercury emissions are lower than previous estimates
- Mercury stocks in biomass strongly constrain wildfire emissions
- Wildfires cause episodic mercury spikes near burned areas despite modest totals
- Postfire vegetation loss produces prolonged changes in land-air mercury fluxes

Authors

Peng Zhang, Tengfei Yuan, Zhengcheng Song, ..., Xin Huang, Minghuai Wang, Yanxu Zhang

Correspondence

yzhang127@tulane.edu

In brief

Wildfires release mercury stored in terrestrial ecosystems, but the traditional emission-factor method overlooks large spatial and temporal variability in biomass mercury content. Using a new atmosphere-land-vegetation coupled model, we find that global wildfire mercury emissions are about three times lower than previous estimates. Although smaller in magnitude, episodic fires can cause strong short-term contamination and long-lasting postfire impact in land-atmosphere mercury exchange.

Zhang et al., 2026, One Earth 9, 101566
March 20, 2026
https://doi.org/10.1016/j.oneear.2025.101566

CellPress

One Earth

CellPress

Article

Global mercury emissions from wildfires are three times lower than existing estimates

Peng Zhang,[1,2,8] Tengfei Yuan,[3,8] Zhengcheng Song,[4] Dong Peng,[2] Mao Mao,[2,3] Yujuan Wang,[5] Shaojian Huang,[2,3] Lu Hu,[6] Fang Li,[7] Xin Huang,[2] Minghuai Wang,[2] and Yanxu Zhang[3,9,*]

[1]School of Environment, Hangzhou Institute for Advanced Study, University of Chinese Academy of Sciences, Hangzhou 310024, China
[2]School of Atmospheric Sciences, Nanjing University, Nanjing 210023, China
[3]Department of Earth and Environmental Sciences, Tulane University, New Orleans, LA 70118, USA
[4]State Key Laboratory of Environmental Geochemistry, Institute of Geochemistry, Chinese Academy of Sciences, Guiyang 550081, China
[5]School of Environmental Science and Engineering, Nanjing University of Information Science & Technology, Nanjing 210044, China
[6]Department of Chemistry and Biochemistry, University of Montana, Missoula, MT 59812, USA
[7]International Center for Climate and Environment Sciences, Institute of Atmospheric Physics, Chinese Academy of Sciences, Beijing 100029, China
[8]These authors contributed equally
[9]Lead contact
*Correspondence: yzhang127@tulane.edu
https://doi.org/10.1016/j.oneear.2025.101566

SCIENCE FOR SOCIETY Mercury pollution is a global environmental concern because it can travel long distances, accumulate in ecosystems, and threaten human health. As wildfires intensify, understanding how much mercury they release has become increasingly important. However, many estimates often rely on simplified assumptions that treat mercury emissions as proportional to burned biomass, ignoring how mercury varies within terrestrial ecosystems. This study uses an advanced atmosphere-land-vegetation coupled model to provide a more realistic assessment of wildfire mercury emissions and their impacts. We find that global emissions are much lower than previously estimated, but individual fire events can still cause short-term local mercury spikes and long-term changes in land-air mercury exchange after vegetation loss. These insights enable more accurate evaluation of mercury risks and support better environmental and public health strategies in a fire-prone future.

SUMMARY

Wildfires reintroduce mercury (Hg) stored in terrestrial ecosystems into the atmosphere, raising concerns about environmental and health risks. Existing estimates rely on emission factors derived from limited observations and assume that Hg emissions scale with burnt biomass. This simplification can bias emissions because it neglects the variability in Hg content and fire intensity. Here, we develop an atmosphere-land-vegetation coupled Hg model to simulate wildfire Hg emissions and postfire impacts for 1995–2014. Our results show that global wildfire Hg emissions are about three times lower than previous estimates, revealing that Hg release is controlled primarily by Hg content rather than burnt biomass. Although these emissions are equivalent to only 10% of global anthropogenic Hg emissions, we find that episodic fires can cause significant short-term local contamination and alter land-atmosphere Hg exchange through a wildfire-vegetation-Hg feedback loop. These impacts warrant greater attention as wildfire risks continue to rise in a warmer future.

INTRODUCTION

The frequency and intensity of wildfires have been increasing in recent decades due to global warming,[1,2] accompanied by the release of various air pollutants.[3,4] Mercury (Hg), one of these pollutants, can be transported over long distances given its high volatility and long atmospheric lifetime.[5,6] Once released into the atmosphere, Hg can be deposited into aquatic ecosystems, where it is methylated by microorganisms into toxic methylmercury, posing significant health risks to humans through the consumption of seafood and rice.[7,8] However, there is still large uncertainty in the estimates of Hg emissions from wildfires,

Please cite this article in press as: Zhang et al., Global mercury emissions from wildfires are three times lower than existing estimates, One Earth (2025), https://doi.org/10.1016/j.oneear.2025.101566

which range from 210 to 1,330 Mg year^{-1}.[9] This is equivalent to roughly 10%–60% of global anthropogenic Hg emissions, making fires an important episodic source that can drive sharp short-term pollution spikes and subsequently enhance downstream methylmercury production and transport.[9,10]

Early studies typically measured atmospheric Hg in smoke plumes using ground-based stations[6,11,12] or aircraft[13–15] away from the fire source, as directly measuring Hg emissions during fire events is highly challenging. Several studies have estimated wildfire Hg emissions by measuring changes in Hg burden in vegetation and soil before and after burning.[16,17] Emission factors (EFs) of Hg are derived from these laboratory and field experiments and then combined with published or diagnostic burned biomass databases to estimate regional or global Hg emissions from wildfires. However, using EFs from localized fire events for large-scale estimates fails to account for spatial variations in terrestrial environments and differences in burning intensity, leading to significant uncertainties.[18,19] In particular, peat fires involve deep combustion and high soil mercury storage, leading to much higher emissions than non-peat fires,[20] yet this distinction is often overlooked in EF-based estimates. Recent studies have sought to estimate wildfire Hg emissions on a continental or global scale by integrating previous EF measurements across different geographic regions and vegetation types.[21–23] However, due to the limited number of EF measurements and inconsistencies in assessment techniques, EF values for the same vegetation type can vary by one to two orders of magnitude between studies.[22] This large variability, raised from different fire conditions, fuel types, and burning phases, combined with sparse spatial and temporal coverage, limits the applicability of current EF datasets to represent global wildfire emissions. Additionally, although the method of estimating emissions using EFs (hereafter referred to as the EF method) is theoretically based on the amount of pollutant released per unit of fuel burned, in practice, the EF of Hg typically relies on generalized or inferred values that do not account for the actual Hg content in region-specific fuels,[22] which is one of the determining factors in the amount of Hg released during burning.[16] This limits the accuracy of Hg emission estimates, particularly in regions with highly variable biomass Hg content, and prevents reliable assessment of wildfire-driven Hg exposure and its environmental impacts. Neglecting postfire changes in vegetation and soil further obscures the long-term influence of fires on land-atmosphere Hg cycling,[24] leaving substantial uncertainties in both regional and global Hg budgets.

Here, we address these uncertainties by applying an atmosphere-land-vegetation coupled Hg modeling framework that overcomes the limitations of EF-based approaches reliant on sparse and non-representative measurements. Unlike the EF method, which assumes that Hg emissions scale with burned biomass, this framework captures nonlinear interactions among fuel Hg content, fire behavior, and land-atmosphere exchange, allowing emissions to emerge directly from underlying biogeochemical processes. Using this coupled model, we quantify global, inter-annual, seasonal, and event-scale wildfire Hg emissions. The model estimates global annual wildfire Hg emissions during 1995–2014 to be 204 ± 121 Mg year^{-1}, which is about three times lower than EF-based estimates. This difference arises because the Hg content in biomass, rather than carbon (C) loss alone, determines the magnitude of emissions. The framework also reveals substantial short-term atmospheric enhancements during fire events, reaching up to 7,000 ppq near fire regions, as well as persistent postfire shifts in land-atmosphere Hg exchange caused by vegetation and soil loss. Together, these findings reduce major observational and methodological gaps in current wildfire Hg assessments and provide a more robust basis for evaluating Hg exposure risks, including short-term spikes in atmospheric Hg levels, alterations to regional Hg cycling, and potential contamination of ecosystems and food chains in a warming and increasingly fire-prone world.

RESULTS

Methods summary

The model integrates the atmospheric Hg model (CAM6-Chem/Hg)[25] and terrestrial Hg model (CLM5-Hg),[26] which are coupled online via the CIME coupler within the Community Earth System Model version 2 (CESM2).[27] It dynamically simulates both within-compartment (atmospheric and terrestrial) cycling and cross-compartment (land-atmosphere) exchange of Hg. We focus on wildfire processes, including non-peat fires and peat fires, where the burned area is influenced by climate and weather conditions, vegetation composition and structure, and human activities.[28] Wildfire Hg emissions are computed based on biomass and peat burning and adjusted by the ratio of satellite-derived to modeled C emissions. The model also tracks changes in vegetation and soil Hg pools following burning, allowing fire-induced losses of canopy, litter, and organic soils to alter postfire gaseous uptake and deposition. This representation captures both the immediate release of Hg during combustion and the long-term shifts in biogeochemical cycling that affect regional land-atmosphere fluxes for months to years.

Lower wildfire Hg emissions

We estimate the mean annual global wildfire Hg emissions during 1995–2014 to be 204 ± 121 Mg year^{-1}, with 72% from non-peat fires and 28% from peat fires. Using the 14 regions defined by the Global Fire Emissions Database (GFED)[29] (Figure 1A), we find that Equatorial Asia (EQAS) is the largest contributor to wildfire Hg emissions (30.8%), followed by Southern Hemisphere Africa (SHAF) (20.0%) and Northern Hemisphere Africa (NHAF) (19.0%) (Figure 1B). The high emissions in SHAF and NHAF are associated with the active wildfires in the region, which account for the largest proportion of burned area (68.6%) globally (Figure 1E). In contrast, EQAS accounts for only 0.6% of the global burned area but contributes disproportionately to the highest regional Hg emissions through extensive peatland burning. When considering only Hg emissions from non-peat fires, EQAS's contribution drops to 4.7% (Figure S1).

Our estimate is significantly lower than previous estimates (612–675 Mg year^{-1}) based on the EF method.[21,22] For comparison, we assign the region-specific EF values compiled by Kumar et al.[21] to different regions and vegetation types (see the methods), resulting in a diagnostic global wildfire Hg emission of 576 Mg year^{-1} (Figure 1C). This value is close to the previous EF-based estimates but about three times higher than our modeled result. Large discrepancies also exist in the spatial distribution of emissions between the two methods (Figure 1D). In

Please cite this article in press as: Zhang et al., Global mercury emissions from wildfires are three times lower than existing estimates, One Earth (2025), https://doi.org/10.1016/j.oneear.2025.101566

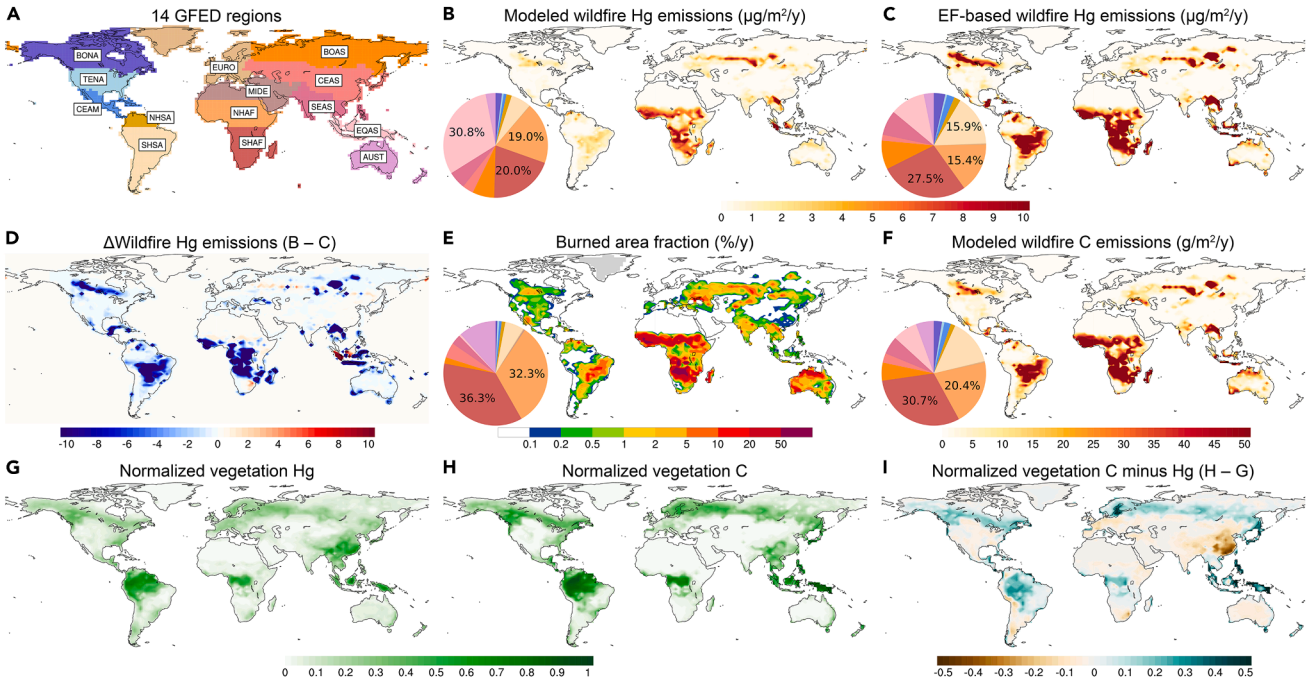

Figure 1. Global distribution of Hg and C emissions from wildfires and their content in vegetation

(A) Map of 14 geographic regions used in this study according to the Global Fire Emissions Database (GFED) (see Table S1 for the full names of the 14 regions).

(B and C) Spatial distribution of annual mean wildfire Hg emissions for the period 1995–2014 estimated by the coupled Hg model and the emission factor (EF) method, respectively.

(D) The absolute difference between (B) modeled emissions and (C) EF-based emissions, i.e., (B) − (C).

(E and F) Spatial distribution of burned area fraction and modeled wildfire C emissions, respectively.

(G and H) Spatial distribution of normalized Hg and C contents in vegetation, respectively.

(I) The absolute difference between normalized (H) C content and (G) Hg content in vegetation, i.e., (H)−(G).

The pie charts in (B), (C), (E), and (F) show the relative contributions of the 14 geographic regions. The colors are consistent with the definitions in (A), and only regions with contributions exceeding 15% are labeled.

the EF-based estimates, SHAF becomes the largest contributor to wildfire Hg emissions (27.5%), followed by Southern Hemisphere South America (SHSA; 15.9%) and NHAF (15.4%). It is noted that EQAS only contributes 10.9% to the total Hg emissions, which is related to the low proportion of wildfire C emissions in this region (7.6%). Overall, the spatial distribution of EF-based wildfire Hg emissions across the 14 regions is highly consistent with that of modeled wildfire C emissions (Figure 1F) (Pearson correlation coefficient $r = 0.97$), indicating a strong correlation between Hg and C emissions obtained from the EF method. In contrast, the correlation between the wildfire Hg emissions and C emissions is much weaker in our model ($r = 0.66$).

The primary distinction between the EF-based approach and our findings stems from the fact that we consider the variations between Hg and C within terrestrial ecosystems. Fuel load, defined as the available biomass for combustion, is one of the main limiting factors for fire occurrence and emissions in the model.[30] However, due to the unique physicochemical processes of Hg (e.g., deposition and redox chemistry), Hg content in soil and vegetation is much higher in contaminated areas than remote regions,[31] leading to large differences between Hg and C contents in biomass. Our model shows that C content in vegetation is relatively high in equatorial and boreal regions, while Hg content is elevated in regions near pollution sources (e.g., East Asia and the Amazon) (Figures 1G and 1H). When wildfires occur, this spatial discrepancy in Hg and C contents in vegetation (Figure 1I) results in differences in the spatial distribution of wildfire Hg emissions estimated by the two methods (Figure 1C). We further conduct a sensitivity simulation by replacing the modeled wildfire Hg emissions with the EF-based diagnostic results at each time step. The results show abnormally high wildfire Hg emissions estimates compared to the available Hg content for combustion in certain grid cells (Figure S2). Australia (AUST) provides a typical example to illustrate this issue: the burned area in AUST accounts for 11.7% of the global total, but its contribution to Hg emissions is relatively small (3.1%) due to the low Hg content in local vegetation. Recent measurements from Australian smoke plumes reveal that local EF values are significantly lower than those from other regions,[32] which have been used as proxies for estimating wildfire Hg emissions in AUST.[33] We argue that EF methods derived from limited measurements or a single fire event are associated with large uncertainties.[19,20] This leads to a tendency to overestimate Hg emissions in major wildfire regions (e.g., SHAF, NHAF, and SHSA) while underestimating them in the vicinity of Hg-contaminated regions [e.g., EQAS and Central Asia (CEAS)]. This discrepancy implies that assessments of wildfire Hg emissions based on the EF method may misrepresent their spatial patterns, thereby affecting our broader understanding of Hg cycling and its environmental risks.

Please cite this article in press as: Zhang et al., Global mercury emissions from wildfires are three times lower than existing estimates, One Earth (2025), https://doi.org/10.1016/j.oneear.2025.101566

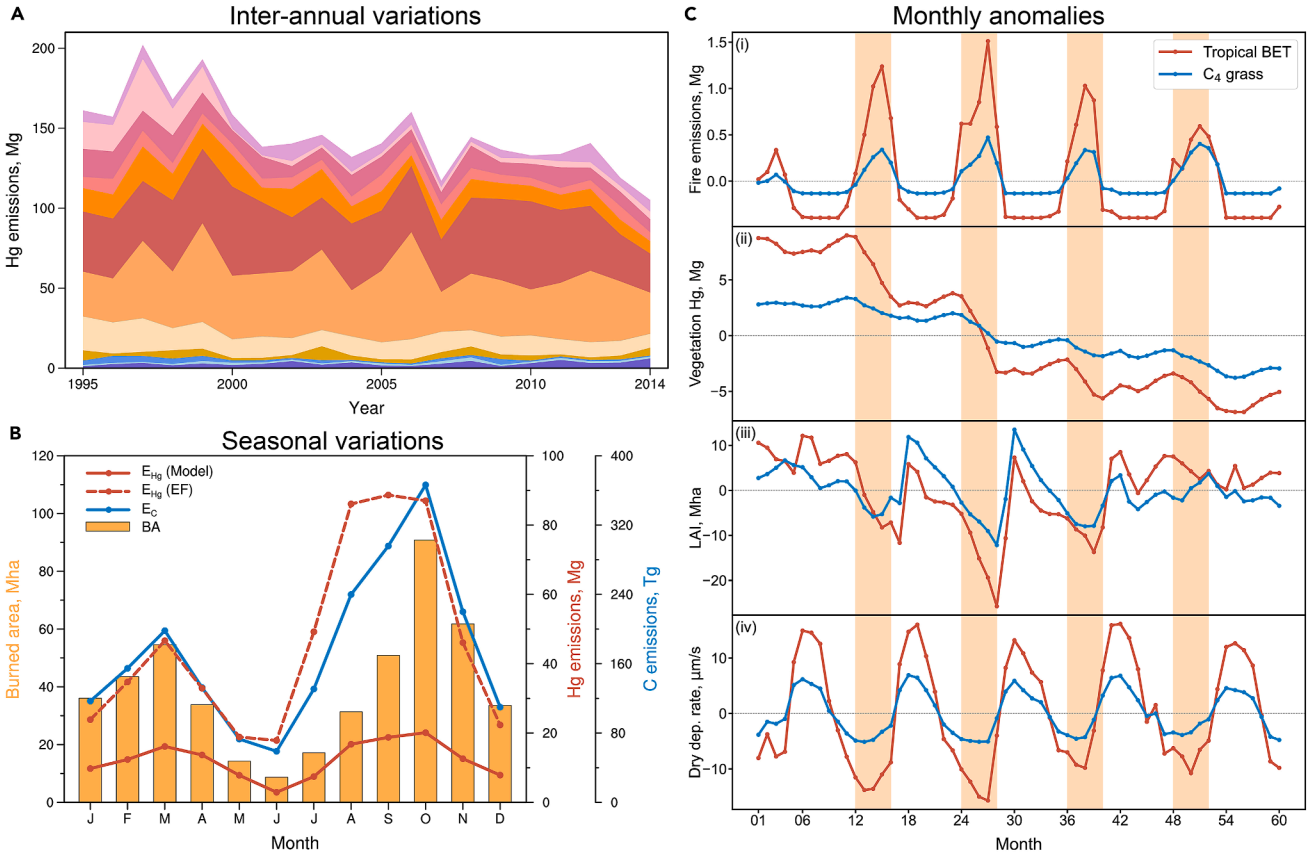

Figure 2. Temporal variations of Hg emissions from non-peat fires and the impact of specific fire events on Hg-related processes

(A) Inter-annual variations of non-peat-fire Hg emissions in 14 regions from 1995 to 2014. The colors correspond to those defined in Figure 1A.

(B) Monthly variations of modeled Hg emissions (solid red line), EF-based Hg emissions (dashed red line), modeled C emissions (solid blue line), and burned area (orange columns) from non-peat fires.

(C) Monthly anomalies of (i) Hg emissions from non-peat fires, (ii) Hg content in vegetation, (iii) Hg dry deposition rate, and (iv) leaf area index (LAI) in an emission hotspot (16°N–24°N, 95°E–105°E) during 2003–2007. The red and blue lines represent tropical broadleaf evergreen trees and C_4 grass, respectively. The orange columns represent periods with wildfires.

Non-peat-fire Hg emissions and postfire impacts

The global Hg emissions from non-peat fires are estimated to be 146 ± 24 Mg year^{-1} and show a significant decreasing trend of 2,973 kg year^{-1} during 1995–2014 (Figure 2A) (non-parametric Mann-Kendall test with a 5% significance level). This variability is similar to the non-peat-fire C emissions (r = 0.91), which also show a significant decreasing trend (Figure S3A). However, inter-annual variations in both vegetation Hg and C contents are negligible at the global or regional scale (Figures S3C and S3D). It indicates that changes in the burned area (mainly in NHAF and SHSA; Figure S3B) lead to the decline in Hg and C emissions from non-peat fires during this period. Meanwhile, the spatial variations in the vegetation Hg and C contents also result in differences in the regions that drive inter-annual changes in emissions. SHAF and NHAF contribute equally to Hg emissions, while SHAF contributes more to C emissions on average (Figures 2A and S3A).

The modeled global Hg emissions from non-peat fires exhibit clear seasonal variations, with a primary peak from August to October and a second peak in March (red solid line in Figure 2B). Similarly, the modeled non-peat-fire C emissions and burned area show comparable seasonal patterns, with peaks in October and March, respectively. However, the seasonal fluctuations of modeled Hg emissions (coefficient of variation [CV] = 43%) are lower than those of C emissions (CV = 53%), burned areas (CV = 58%), and EF-based Hg emissions (CV = 58%), reflecting different underlying processes for Hg and C emissions. These peaks in burned area coincide geographically with meteorological factors such as high surface temperatures, low precipitation, and low surface relative humidity (Figure S4), which drive the occurrence and extent of fire activity. These weather controls on wildfire activity have been widely examined in previous studies.[34,35] However, the magnitude of Hg released from a given fire is primarily determined by the Hg content in vegetation and soils, which sets an upper bound on emissions. As a result, even under similar fire intensities or burned areas, Hg emissions can differ substantially across regions depending on local terrestrial Hg stocks. It is noted that the modeled Hg emissions from non-peat fires remain elevated from August to October, with low month-to-month variability (<2 Mg month^{-1}; Figure 2B). However, the dominant region for Hg emissions shifts from Eurasia (43.3%) in August to Africa (68.0%) in October,

Please cite this article in press as: Zhang et al., Global mercury emissions from wildfires are three times lower than existing estimates, One Earth (2025), https://doi.org/10.1016/j.oneear.2025.101566

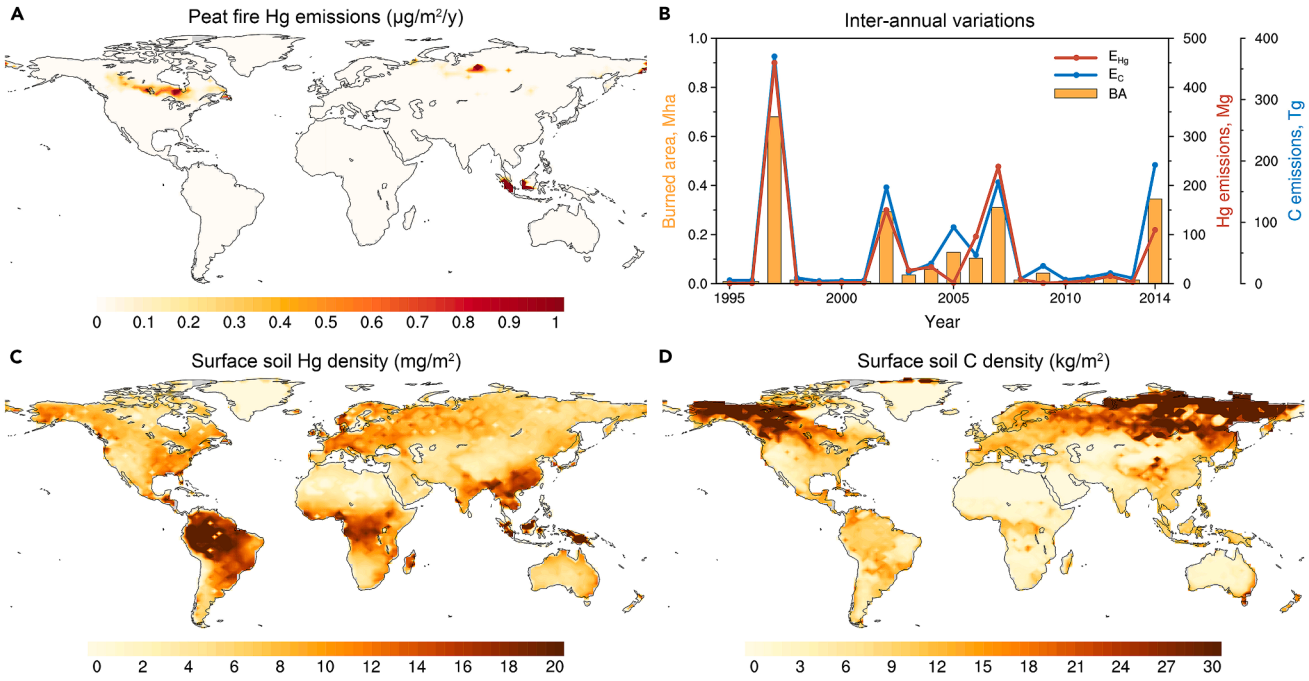

Figure 3. Spatial and temporal distribution of Hg emissions from peat fires

(A) Global distribution of annual mean peat fire Hg emissions.

(B) Inter-annual variations of Hg emissions (red line), C emissions (blue line), and burned area (orange columns) from peat fires from 1995 to 2014.

(C and D) Global distribution of Hg density and C density in surface soil (~1 m), respectively.

while Africa consistently dominates the C emissions during this period (Figure S5). These discrepancies can also be attributed to the spatial differences in Hg and C contents in vegetation, highlighting the temporal decoupling of Hg and C emissions from fires.

We further investigate the postfire impacts on atmospheric and terrestrial Hg cycling in an emission hotspot in Southeast Asia (16°N–24°N, 95°E–105°E), where the vegetation is dominated by tropical broadleaf evergreen trees (BETs) and C_4 grass. We find that with each wildfire event (orange columns in Figure 2C), Hg stored in vegetation rapidly decreases due to biomass burning, accompanied by substantial Hg release into the atmosphere (Figures 2C-i and 2C-ii). Specifically, Hg emissions and the reduction of vegetation Hg content per unit of burned area from tropical BETs were approximately two times higher than those from C_4 grass, reflecting differences in emission intensity across vegetation types.[36] Additionally, we find an interesting fire-vegetation-Hg feedback loop. The fire events lead to substantial vegetation biomass loss, reducing the leaf area index (LAI) of both tropical BETs and C_4 grass (Figure 2C-iii), which in turn affects the dry deposition rate of atmospheric Hg (Figure 2-iv) and weakens the ability of vegetation to act as an Hg sink in the postfire periods. Taking the second fire event as an example, we find that the LAI of tropical BETs and C_4 grass decreased by 0.5% and 1.3%, respectively, compared to pre-fire levels. The Hg dry deposition rate also decreased by 1.8% and 2.7%, respectively. Although these changes are not statistically significant at the 95% confidence level due to the limited sample size, the consistent direction of changes across multiple fire events supports the mechanistic link between vegetation disturbance and atmospheric Hg cycling.

Hg emissions from peat fires

The modeled Hg emissions from peat fires are 58 ± 112 Mg year^{-1} during 1995–2014 with drastically different spatial distributions (Figures 3A and S1A). Peat fire Hg emissions account for 28% of the total wildfire Hg emissions, despite peatlands covering only about 3% of the Earth's land surface.[37] During the study period, a dominant portion of peat fire Hg emissions is concentrated in EQAS (96.8%), followed by boreal North America (BONA; 1.7%) and boreal Asia (BOAS; 1.5%). The spatial distribution of C emissions from peat fires shows a slightly different pattern, with EQAS, BONA, and BOAS contributing 91.5%, 5.8%, and 2.7%, respectively (Figure S6). This decoupling of Hg and C emissions from peat fires is mainly caused by the spatial differences in Hg and C contents in surface soils (Figures 3C and 3D). Hg content in surface soils is higher in temperate and tropical regions due to human activities and atmospheric deposition,[38] whereas soil organic carbon is predominantly concentrated in the northern high latitudes, where low decomposition rates prevail.[39]

We find a drastic inter-annual variability for Hg emissions from peat fires (red solid line in Figure 3B). Specifically, there are 4 years (1997, 2002, 2007, and 2014) when Hg emissions exceeded 100 Mg year^{-1}, while emissions in most other years were much lower (<10 Mg year^{-1}). The inter-annual variability in Hg emissions from peat fires is broadly consistent with that of C emissions (r = 0.94). In both 1997 and 2002, Hg emissions

Please cite this article in press as: Zhang et al., Global mercury emissions from wildfires are three times lower than existing estimates, One Earth (2025), https://doi.org/10.1016/j.oneear.2025.101566

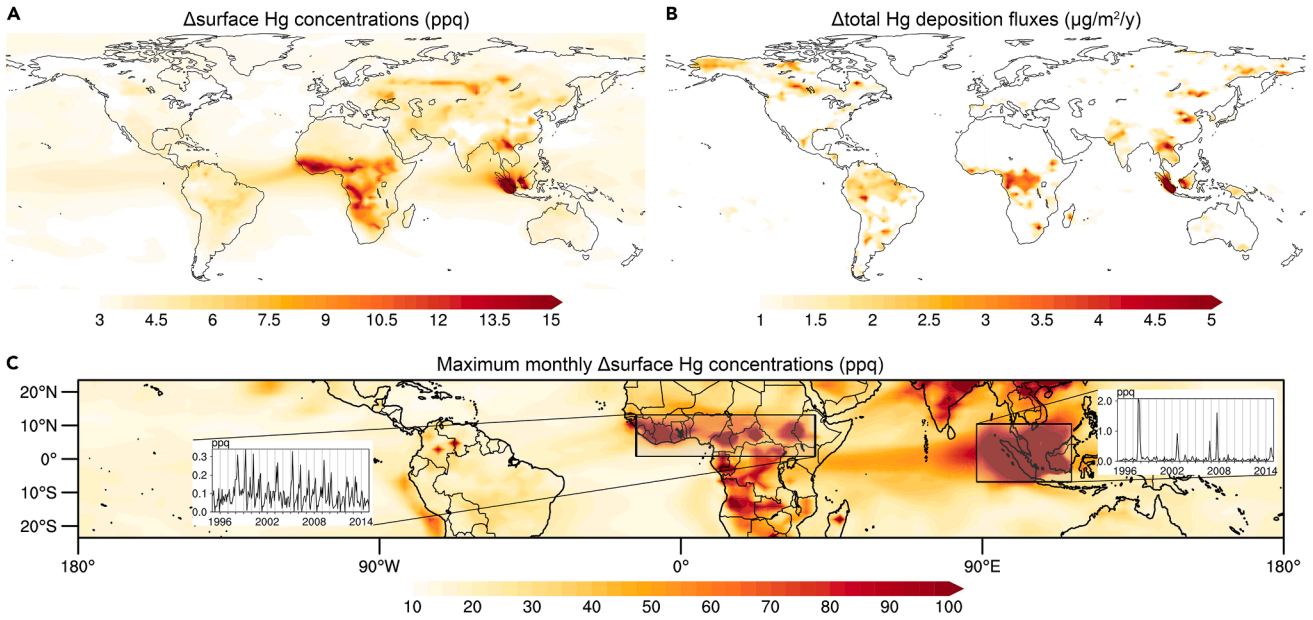

Figure 4. Effects of wildfire Hg emissions on atmospheric Hg concentrations and deposition

(A and B) Global distribution of wildfire-induced multi-year average changes in (A) surface atmospheric Hg concentrations and (B) total Hg deposition fluxes. (C) Distribution of maximum monthly atmospheric Hg concentrations changes in the tropics and monthly time series for selected regions.

from peat fires were more than twice those from non-peat fires, despite the burned area being less than 1% of that of non-peat fires. This indicates an extremely high Hg emission intensity in peatlands. The particularly high Hg emissions in 1997 are concentrated in Indonesia, driven by the drought and deforestation associated with the severe El Niño event in 1997–1998, which also led to substantial C emissions during this extreme peat fire event.[40] Friedli et al.[22] also reported high Hg emissions in the EQAS region in 1997 (>700 Mg) using the EF method, which was similar to our estimate (652 Mg), but their approach cannot quantify the relative contributions of peat and non-peat fires. The seasonal variations of Hg emissions from peat fires differ slightly from those of non-peat fires, with emissions showing a single peak and being primarily concentrated between July and October (Figure S7). This seasonal emission pattern is largely driven by human activities, particularly peatland clearing for agriculture or industry during the dry season.[40] Furthermore, although boreal peatlands, a major global Hg sink, do not show high Hg emissions in our simulation during the study period, they may face significant emission risks[20] as wildfires expand northward with future global warming.[41]

Impact on atmospheric Hg levels and deposition

We quantify the impact of wildfire Hg emissions on atmospheric levels and deposition by comparing model simulations with and without wildfire Hg emissions. Globally, wildfires result in an average increase of 2.5% in surface Hg concentrations (+3.7 ppq) and 2.9% in total atmospheric Hg mass (+130.2 Mg). The spatial distribution of elevated surface Hg concentrations strongly correlates with wildfire Hg emission hotspots (r = 0.89). These increases are concentrated in the tropics (23.5°S–23.5°N), where surface Hg concentrations rise 40.5% higher than in extratropical regions (Figure 4A). Our model indicates that Indonesia has the largest increase (>190 ppq), primarily driven by peat fire Hg emissions, while the increase in other regions is mainly from non-peat fires. In contrast to the spatial distribution of anthropogenic Hg emissions, wildfire Hg emissions are higher in the Southern Hemisphere than in the Northern Hemisphere, decreasing the interhemispheric gradient of surface Hg concentrations (defined as the North-South concentration ratio) from 1.36 to 1.35. The elevated atmospheric Hg levels from wildfires in turn enhance atmospheric Hg deposition, leading to an average increase of 202.2 Mg year^{-1} (Figure 4B). Although Hg emitted from wildfires can undergo long-range transport through the atmosphere, a considerable portion of the increased atmospheric Hg deposits back near the fire sources (r = 0.63), as tropical regions serve as important sinks for atmospheric Hg. Specifically, the increase in atmospheric Hg deposition attributable to wildfire emissions is higher in the tropics (119.9 Mg year^{-1}) compared to extratropical regions (82.2 Mg year^{-1}).

Results at the monthly scale further highlight the local and episodic impact of wildfire emissions on atmospheric Hg concentrations. These episodic emissions contribute to acute spikes in atmospheric Hg levels, with the maximum monthly increase averaged over the tropics exceeding the multi-year average by about 311%. More specifically, over 10% of the tropical region experiences a monthly maximum increase exceeding 50 ppq, with the highest grid-level increase surpassing 7,000 ppq (Figure 4C). There are also clear regional differences in the impact of wildfires on Hg concentrations, with Southeast Asia showing stronger episodic fluctuations compared to equatorial Africa at the monthly scale (shaded area in Figure 4C). Although wildfire Hg emissions are an order of magnitude lower than the anthropogenic sources, the episodic nature of wildfire emissions leads to sharp, localized spikes that may have a disproportionate short-term impact on ecosystems and human health.

Please cite this article in press as: Zhang et al., Global mercury emissions from wildfires are three times lower than existing estimates, One Earth (2025), https://doi.org/10.1016/j.oneear.2025.101566

DISCUSSION

Implications

Existing estimates of wildfire Hg emissions are highly uncertain due to a reliance on limited EF measurements that do not capture spatial variability in biomass Hg content, fire severity, and postfire changes in vegetation and soil. Here, we use a coupled atmosphere-land Hg model to provide process-based emission estimates that integrate biomass Hg content, fire-vegetation feedbacks, and postfire adjustments. Our simulation results indicate that global Hg emissions from wildfires are significantly lower than EF-based estimates,[21,22] highlighting that biomass Hg content, rather than simply burnt biomass, dominates Hg emission. By explicitly accounting for spatial heterogeneity, wildfire-vegetation-Hg feedbacks, and postfire adjustments, our model reduces major uncertainties in emission estimates and improves mechanistic understanding of Hg cycling. This enhanced understanding can inform more accurate assessments of Hg exposure risks and guide evaluations of land-use and fire management impacts on global Hg cycling. Furthermore, the lower estimate of wildfire Hg emissions suggests that the atmospheric lifetime of Hg is likely slightly longer than previously believed (6.6 vs. 5.3 months[25]), given the constraint of the observed atmospheric Hg levels. Alternatively, current global emission inventories may underestimate other Hg sources by about 400 Mg year^{-1}, including both anthropogenic emissions and re-emissions from soils and oceans, the estimate of which also bears large uncertainties.[42]

The very limited observations of the EF of Hg have constrained the accurate representation of Hg content in biomass when using the EF method. Based on comparisons with our simulation results, we emphasize the need to increase field observations and experimental measurements of Hg's EF in regions where wildfire Hg emissions are the largest or are highly variable. In particular, Central Africa, tropical South America, and Southeast Asia emerge from our analysis as priority areas due to their frequent and intense fires and the substantial contribution of biomass burning to regional Hg emissions. Improvements in EF-based approaches should also prioritize refining EF classifications according to vegetation type and geographic region, enhancing the spatial and temporal resolution of fuel load and combustion completeness data, and incorporating postfire vegetation feedback mechanisms. Together, these advancements would significantly enhance the accuracy and reliability of Hg emission estimates from wildfires. This focus on EF uncertainty is also relevant for other pollutants, such as Pb, Cd, and semi-volatile organic compounds, which share similar interactions with vegetation and soils and may be remobilized by wildfires, suggesting that analogous process-based assessments could improve emission estimates for multiple contaminants.

Climate change alters the frequency and intensity of wildfires, leading to changes in vegetation cover and C release, which provides a feedback effect on the global and regional climate through a complex wildfire-vegetation-climate feedback loop.[43] Using the coupled model, we identify an additional wildfire-vegetation-Hg feedback loop. Wildfires directly increase atmospheric Hg sources through biomass burning and subsequent soil emissions while also indirectly reducing atmospheric Hg sinks by affecting vegetation. These combined effects exacerbate atmospheric Hg pollution. The postfire impacts, which are crucial but often overlooked in atmospheric and terrestrial Hg cycling studies,[24] should be considered when assessing the full impact of wildfires.

Although our modeling results indicate that current Hg emissions from wildfires are relatively low, the episodic nature of Hg emissions from wildfires is evident in the occurrence of large spike years, which significantly deviate from typical emission levels. For instance, Hg emissions from the 1997 peat fire event were estimated to be about one-third of global anthropogenic Hg emissions, posing a significant short-term risk of localized Hg contamination. More recently, a series of extreme wildfire events have occurred globally, with record-breaking local wildfire burned area and emissions (e.g., AUST in 2019–2020, the western United States and Siberia in 2020 and 2021, and Canada in 2023–2024).[44] Hg emissions from such extreme events are expected to have large implications for the global Hg cycle, and our model provides an effective tool for assessing these events and their potential impacts. Furthermore, the increasing frequency and intensity of wildfires driven by climate change,[2] along with their shifting spatial patterns,[36] could pose a more prominent impact on global terrestrial Hg stocks (e.g., forests and peatlands) and the atmospheric Hg pools in the coming decades. The burned area is projected to show a significant positive trend primarily in regions such as the Amazon, northwest Eurasia, and Southeast Asia,[45,46] which also coincide with areas of high terrestrial Hg content. In summary, while previous studies have predominantly focused on ozone, carbon monoxide, volatile organic compounds, and particulate matter contained in wildfire smoke,[47–49] the health impacts of Hg triggered by wildfires cannot be overlooked and warrant further investigation.

Uncertainties

Potential uncertainties exist in our model results. Firstly, accurately describing wildfire processes is crucial for emission estimates. The fire module in CLM5 has been extensively evaluated for simulating the burned area and wildfire emissions.[50–52] Uncertainties remain in the parameterization of specific fire processes, such as deforestation and peat fires in boreal tundra, primarily due to a lack of observations and mechanism analyses.[28,30] Compared to the latest GFED5 estimate,[53] CLM5, like most other wildfire models, lacks adequate representation of small fires, resulting in an underestimation of the burned area. Uncertainties also exist in the parameterization of wildfire emissions, such as the use of fixed combustion completeness factors that do not account for potential variations in environmental conditions. In reality, combustion completeness can vary with fire intensity, fuel moisture, and vegetation type, which may affect the absolute magnitude of simulated emissions. For the dominant case of foliage combustion, combustion completeness is generally set between 0.7 and 0.85,[30] and such variation is not expected to substantially affect the overall emission estimates. Additionally, the parameterization for peat wildfire emissions is largely based on a single event, which may lack representativeness over a longer period.[28] Future modeling efforts would benefit from more in-depth analyses of fire mechanisms and a broader range of observations.

Secondly, the GFED4s fire emissions inventory, while widely used in global fire and atmospheric modeling,[54] contains

Please cite this article in press as: Zhang et al., Global mercury emissions from wildfires are three times lower than existing estimates, One Earth (2025), https://doi.org/10.1016/j.oneear.2025.101566

inherent uncertainties that can influence the accuracy of derived Hg emission estimates. One key source of uncertainty stems from the satellite detection of small fires, especially before the MODIS era (pre-2000), when GFED relied on lower-resolution sensors (e.g., Along Track Scanning Radiometer).[29] Additional uncertainty arises from assumptions in fuel consumption, with limited ground-based validation hampering formal error assessment.[29] Notably, GFED5 estimated a 61% higher burned area than GFED4s due to its improved small fire detection algorithm.[53] However, emission products based on GFED5 have not yet been released. Overall, GFED4s has an estimated uncertainty of ±20%–25% (1σ), which could be higher in regions dominated by small fires or organic soils.[55]

Thirdly, there is uncertainty in the representation of atmospheric Hg migration into land, which serves as the primary source of Hg in terrestrial ecosystems and is therefore highly relevant for estimating Hg emissions from wildfires. The simulation results for total Hg vegetation uptake are generally consistent with dataset-based estimates, with overall uncertainty estimated to be around 17% in the CLM5-Hg-only analysis.[56] Uncertainties arise in the parameterization of vegetation uptake, particularly regarding stomatal resistance and biological reactivity. Using fixed biological reactivity may also lead to discrepancies between modeled results and observations for different deposition types.[57] An additional limitation stems from the model's omission of Hg uptake through plant roots, potentially leading to a systematic underestimation of vegetation Hg accumulation. In contrast to the uncoupled model, which either prescribes land emissions or neglects vegetation and soil feedback, the coupled model allows vegetation and soil to act as sources or sinks depending on the atmospheric and ecosystem conditions. This improves mechanistic representation but also introduces uncertainties in land-atmosphere exchange, particularly in vegetation uptake, soil storage, and postfire recovery. More observations, especially those focused on various vegetation types, along with advancements in observational techniques, such as isotopic methods[58] and micrometeorological techniques,[59] are essential to reduce these uncertainties.

Fourthly, the migration and transformation of Hg between different vegetation tissues remain poorly understood and are subject to gaps in scientific knowledge and observations.[60,61] For instance, the chemical transformation and re-emission rates of absorbed Hg within plants can vary widely depending on vegetation type, physiological status, and environmental conditions. Hg dynamics in soil and vegetation are constrained by limited Hg-specific data, with many CLM5-Hg parameters adapted from C-related parameters, leaving uncertainties in their environmental and physiological dependencies unresolved and computationally difficult to quantify.[26] In this study, we utilize the well-studied litterfall Hg flux[62–64] as a constraint on vegetation Hg, leveraging the advanced prognostic capabilities of the CLM5 model in vegetation phenology[65] to reduce the model uncertainties.

Fifthly, the atmospheric Hg process significantly influences the Hg exchange flux between the land and atmosphere, and its simulation is subject to large uncertainties due to factors such as atmospheric transport and redox chemistry.[66] Our model employs different chemical mechanisms compared to those newly proposed by Shah et al.,[67] yet it shows reasonable agreement with observational data. The overall uncertainty in atmospheric processes can be quantified by the normalized root-mean-square error between the modeled and observed ground-level total atmospheric Hg levels (9%). Since the spatiotemporal variability in wildfire Hg emissions is influenced more directly by the local Hg content in vegetation and soil, as well as the specific characteristics of each fire event (e.g., fuel load, fire intensity, and meteorological conditions), uncertainty from atmospheric chemical mechanisms plays a comparatively minor role in determining emission estimates.

METHODS

The coupled Hg model description

The atmospheric and terrestrial components of the coupled model are based on CAM6-Chem/Hg[25] and CLM5-Hg,[26] respectively. The atmospheric component simulates the emissions, chemistry, transport, and depositions of three main Hg species: gaseous elemental Hg (Hg^0), reactive gaseous Hg (Hg^2), and particulate-bound Hg (Hg^P). Specifically, re-emissions from land, including wildfire emissions, Hg^0 vegetation re-emissions, Hg^{II} (Hg^2 and Hg^P) photoreduction, and soil decomposition, are calculated online by the terrestrial component, while anthropogenic emissions, other natural emissions (e.g., geological and snow emissions), and marine re-emissions follow CAM6-Chem/Hg.[25] The redox chemical mechanism for atmospheric Hg remains unchanged, with adjustments made to the oxidation rates by Br and OH (Table S2) to align with atmospheric Hg observations. We do not adopt the new Hg chemical mechanism proposed by Shah et al.[67] due to its discrepancies in simulating seasonal variations of atmospheric Hg compared to observations.[57,67] The modeling of atmospheric Hg depositions includes Hg^0 dry deposition and Hg^{II} dry and wet depositions. The dry deposition velocities of Hg^0 and Hg^2 are calculated online in CLM5 using the multiple-resistance approach.[68,69] The wet deposition of Hg^2 is treated like other soluble gas-phase species, considering both in-cloud and below-cloud processes.[68] Dry and wet removal of Hg^P follows the same scheme as other aerosol species in CAM6-Chem.[70]

The terrestrial component simulates the Hg cycle in vegetation and soil. The fixed atmospheric Hg^0 concentrations and Hg^{II} depositions previously used as upper boundary conditions in CLM5-Hg are now replaced by the online-calculated dynamic Hg^0 and Hg^{II} deposition fluxes at each time step. The atmospheric Hg^0 dry deposition flux previously simulated by CAM6-Chem/Hg (~1,000 Mg $year^{-1}$) is likely underestimated by a factor of two or three.[59,61] Feinberg et al.[57] reported a global Hg^0 dry deposition flux of 2,276 Mg $year^{-1}$ by adjusting the biological reactivity (f_0) of Hg^0 in GEOS-Chem. However, such standalone atmospheric Hg models have inherent limitations in simulating land-atmosphere feedback caused by changes in deposition. In this study, the f_0 and stomatal resistance (R_s) of Hg^0 are adjusted (Table S3) to match the available dry deposition measurements. We assume that 70% of the Hg^0 dry deposition is incorporated into the leaf Hg pool and the rest is re-emitted to the atmosphere.[71] Assimilation of Hg^{II} dry deposition can occur through non-stomatal uptake via cuticles, but the specific mechanisms and proportions remain unclear,[61,72] and we assume that 10% of the Hg^{II} dry deposition is incorporated into the leaf Hg

Please cite this article in press as: Zhang et al., Global mercury emissions from wildfires are three times lower than existing estimates, One Earth (2025), https://doi.org/10.1016/j.oneear.2025.101566

pool. The remaining Hg^{II} dry deposition, along with Hg^{II} wet deposition, is incorporated into the surface soil Hg pool, from which 30% is assumed to be re-emitted to the atmosphere as Hg^0 through photoreduction and other processes.[73,74] We do not consider Hg dynamics in plant organs and tissues due to insufficient knowledge of the mechanisms involved.[60,72] The leaf Hg pool is linked with the soil Hg through the vegetation phenology process. Soil Hg is represented by seven pools, including one coarse woody debris pool, three litter pools, and three soil organic matter pools. The transfer processes between these Hg pools follow the same coupling and dynamics as soil C pools in CLM5.[26] The parameterization of Hg^0 emissions from soil decomposition is based on the C decomposition emissions and the Hg/C emission ratio (0.05 μg Hg g^{-1} C) derived from a laboratory study.[75]

The exchange of Hg fluxes between the atmospheric and terrestrial components is conducted through the CIME coupler,[27] which includes the atmospheric Hg depositions and the land re-remissions as described above. The simulation operates at a 30-min temporal resolution and a horizontal resolution of 1.9° latitude × 2.5° longitude for both components. To improve computational efficiency, we first use the Global Soil Wetness Project (GSWP3) forcing dataset meteorology (1980–1989) and fixed monthly mean atmospheric Hg deposition fields from CAM6-Chem/Hg to drive CLM5-Hg for 70 years. Vegetation Hg pools were initialized from zero, while soil Hg pools were initialized from the observation-based dataset of Wang et al.[38] Given the large soil Hg reservoir (~740 Gg) relative to annual atmospheric deposition (~4 Gg), the spin-up does not change the soil pool significantly but does enable a quasi-steady state for vegetation with respect to present-day inputs, although some regional biases may remain in areas with strong historical-present differences. The results from the final year are then used to initialize the coupled model. We run the coupled model in a free-running configuration with specified sea surface temperatures for 25 years (1990–2014). The first 5 years are used for the spin-up of atmospheric Hg pools, and the last 20 years (1995–2014) are used for analysis. We do not extend the simulation beyond 2014 due to limitations in the model input data (e.g., historical emissions, land-use and land-cover change, population density, and lightning frequency), which are important parameters for fire simulation.[28,30]

Parameterization of Hg emissions from wildfires

The fire module in CLM5 includes non-peat fires (i.e., agricultural fires in cropland, deforestation and degradation fires in tropical closed forests, and other fires outside cropland and tropical closed forests) and peat fires. Calculation of the burned area for different types of fire considered the effect of climate and weather conditions, vegetation structure and composition, and human activities (see Li et al.[28,30] for details). Following the original non-peat-fire C emission scheme in CLM5, Hg emissions (E_{Hg}) from the non-peat fires are calculated as

$$E_{Hg,i} = BA_i \cdot D_{Hg,i} \cdot CC_i, \quad \text{(Equation 1)}$$

where i represents 78 plant functional types (PFTs) and BA, D_{Hg}, and CC are non-peat-fire burned area, vertical integration density of Hg in vegetation, and combustion completeness (see Table 2 in Li et al.[30] for details), respectively. Since this scheme accounts for the dynamic changes in Hg content within biomass, it provides a more realistic estimate of wildfire Hg emissions than the EF method mentioned above.

The Hg emissions (E_{Hg}) based on the EF method are calculated as

$$E_{Hg,i} = EF_i \cdot \frac{E_{C,i}}{CF}, \quad \text{(Equation 2)}$$

where EF is the Hg EFs, E_C is the non-peat-fire C emissions simulated in the model, and CF (=0.45) is a conversion factor from dry matter to carbon. The values of EF are categorized based on the PFTs in CLM5 and are consistent with those used in the study by Kumar et al.[21]

To our knowledge, Kohlenberg et al.[76] is the only study to date that has demonstrated the relationship between emissions and soil stocks of Hg and C during peat burning in laboratory experiments. Here, we incorporate this relationship into the original peat fire C emission scheme[28] to simulate Hg emissions during peatland burning:

$$E_{Hg} = c \cdot D_{Hg}/D_C \cdot E_C \quad \text{(Equation 3)}$$

$$E_C = \begin{cases} a_1 \cdot BA \cdot D_C, & \text{tropical peat fires} \\ a_2 \cdot BA, & \text{boreal peat fires} \end{cases}, \quad \text{(Equation 4)}$$

where D_{Hg} and D_C are the vertical integration density of Hg and C in soil, respectively; E_C and BA are modeled C emissions and burned area from peat fires, respectively; c (=0.71) is a modified constant for Hg based on the experiments of Kohlenberg et al.[76]; and a_1 (=0.18) and a_2 (=2.2 kg m^{-2}) are constants used in the original fire scheme.[28]

In our simulations, all wildfire Hg emissions are assumed to be in the form of Hg^0, consistent with previous observations showing that Hg^0 accounts for the vast majority of Hg released during biomass burning.[14]

Post-processing of wildfire Hg emissions

Given the free-running configuration used to run the coupled model in this study, we use the satellite-based GFED4s fire product[29] to constrain the model's simulation of wildfire activities. Specifically, we calibrate the modeled wildfire C emissions for 14 GFED regions every 5 years based on wildfire C emission data from GFED4s. It should be noted that since GFED4s data are only available from 1997 onward, we use the average scaling factors from 1997–1999 to adjust model outputs for the first 5-year period (1995–1999). The correlation between the calibrated inter-annual variability of wildfire C emissions and GFED4s is thus improved from 0.39 to 0.72. These scaling factors are then applied to the modeled wildfire Hg emissions, providing a more realistic estimate of present-day wildfire Hg emissions:

$$E^{Cal}_{Hg,j,t} = E^{Mod}_{Hg,j,t} \cdot \frac{\overline{E^{Mod}_{C,j,t}}}{\overline{E^{GFED}_{C,j,t}}}, \quad \text{(Equation 5)}$$

where j represents 14 GFED regions; t represents the calibration time period, with a 5-year interval between each calibration; and E^{Cal}, E^{Mod}, and E^{GFED} are calibrated, modeled, and GFED4s emissions, respectively. Importantly, this correction is implemented as a post-processing step. It only modifies the flux of

Please cite this article in press as: Zhang et al., Global mercury emissions from wildfires are three times lower than existing estimates, One Earth (2025), https://doi.org/10.1016/j.oneear.2025.101566

wildfire Hg emissions passed to the atmosphere, without altering the internally simulated vegetation and soil Hg pools. The Hg stocks in fuels and their depletion during fire events remain governed by the model's prognostic fire occurrence, intensity, and severity. Such region-specific scaling approaches have also been employed in previous studies to reconcile modeled fire emissions with satellite-based constraints.[77,78]

Model validation

Observations of wildfire Hg emissions are typically scarce and unevenly distributed, showing significant differences across fire intensities and types. Additionally, variations in observational methods and timescales between different studies further complicate model validation. Therefore, we use the robust atmospheric and terrestrial observations to constrain the coupled model in this study.

In the atmospheric component, observations of atmospheric Hg concentrations have been successfully conducted for decades through various regional and global networks and are widely used to constrain atmospheric Hg models. We first compare the modeled surface concentrations of atmospheric total gaseous mercury (TGM; the sum of Hg^0 and Hg^2) with available observations. The simulated global annual mean surface concentration of TGM is 1.29 ng m^{-3} STP (standard temperature and pressure; p = 1,013 hPa, T = 273 K), which aligns well with observations across 91 ground-based sites worldwide (coefficient of determination [R^2] = 0.78, root-mean squared error [RMSE] = 0.42 ng m^{-3} STP) (Figure S8A). Importantly, the observed gradient of Hg concentrations between the Northern and Southern Hemispheres[79] is effectively captured by the model (Figure S8B), providing a reliable basis for assessing the contributions of wildfire emissions to global Hg distribution.

In addition to comparing the spatial distribution of TGM concentrations with observations, their seasonal variability is also an important constraint for atmospheric mercury modeling. We compare the simulation results of the coupled model and CAM6-Chem/Hg-only with observations in the northern mid-latitudes (NMLs) and the Southern Hemisphere (Figure S9). Overall, the coupled model shows higher accuracy in simulating observed seasonal variations of surface TGM concentrations in the NML (R^2 = 0.21, RMSE = 0.27 ng m^{-3} STP) compared to CAM6-Chem/Hg-only (R^2 = 0.10, RMSE = 0.29 ng m^{-3} STP). This may be due to the coupling of terrestrial Hg processes improving the modeling of atmospheric Hg concentrations. A previous study suggested that terrestrial vegetation controls seasonal variations in atmospheric Hg concentrations, particularly in the Northern Hemisphere.[80] It is noted that the coupled Hg model tends to overestimate surface TGM concentrations during the winter months in both hemispheres. The overestimation in the Southern Hemispheres may stem from several factors: limited observational coverage (5 sites), uncertainties in oceanic Hg^0 emissions and their seasonal cycle,[81] less-constrained Br concentrations affecting oxidation rates,[67] and underestimated inter-site variability due to model resolution.

Another important atmospheric constraint is Hg deposition, where dry deposition processes serve as a major source of Hg for terrestrial vegetation, significantly influencing the Hg emissions during wildfires. We compare the modeled Hg^0 dry deposition velocities with compiled diagnostic values from litterfall, total foliar uptake, and micrometeorological measurements (Figure S10). The modeled velocities are higher than the observations at litterfall (normalized mean bias [NMB] = 35%, R^2 = 0.44) and foliar uptake sites (NMB = 63%, R^2 = 0.10) but agree well with micrometeorological measurements (NMB = −8%, R^2 = 0.90), which are regarded as a more accurate proxy for total Hg^0 vegetation uptake.[59] Based on these velocities, we obtain a global total Hg^0 dry deposition flux of 2,830.8 Mg $year^{-1}$, which is about 2.8 times higher than the CAM6-Chem/Hg-only estimate but consistent with a recent bottom-up approach estimate of 2,705 ± 504 Mg $year^{-1}$.[64] The modeled Hg^{II} wet deposition is compared with observations in three regions (Figure S11). Compared to CAM6-Chem/Hg-only, the coupled model improves the simulation of Hg^{II} wet deposition in East Asia (NMB = −27% vs. −32%, RMSE = 9.9 vs. 15.4 μg m^{-2} $year^{-1}$), whereas its performance degrades in North America when compared to observations (NMB = −36% vs. −22%, RMSE = 4.2 vs. 3.0 μg m^{-2} $year^{-1}$). This bias mainly reflects enhanced Hg^0 dry deposition, which reduces the Hg^0 available for oxidation. Field evidence shows that vegetation Hg^0 uptake dominates terrestrial inputs (60%–90%),[61] making Hg^0 a more critical constraint for land-atmosphere exchange than Hg^{II} wet deposition. Remaining discrepancies likely stem from incomplete Hg redox chemistry and missing ocean feedbacks. Additionally, the coupled model shows higher accuracy in modeling Hg^{II} wet deposition flux globally compared to the results of Feinberg et al.,[57] which do not account for terrestrial feedbacks associated with the large increase in Hg^0 dry deposition. The atmospheric lifetime of TGM against depositions is 6.6 months in the coupled model, which falls within the range of 4–7 months estimated in previous studies.[67,81,82]

Compared to atmospheric observations, terrestrial Hg observations are scarce and have limited geographic coverage, mainly due to less-established technology and the high spatial heterogeneity of soils. Here, we use observed Hg concentrations in litterfall and soil to constrain the terrestrial component. The simulated mean litterfall Hg concentrations (63.8 ng g^{-1}) are about 20% higher than the observations (Figure S12). The modeled global total litterfall Hg flux is 1,201.1 ± 21.7 Mg $year^{-1}$, which falls within the range of observationally constrained estimates (1,100–1,497 Mg $year^{-1}$) (see Zhou and Obrist[64] and references therein). The modeled Hg concentrations in soil are evaluated by high-resolution observations in topsoil (upper 20 cm) from the United States and Europe. We find that the modeled mean topsoil Hg densities (5.8 ± 2.2 mg m^{-2}) are slightly lower than the observations (6.3 ± 2.3 mg m^{-2}), with the discrepancy reduced after excluding contaminated sites (Figure S13). The model simulates a global total mass of Hg in the topsoil of 739.1 Gg, which represents about two-thirds of the total soil Hg pool and falls within the range estimated based on stable Hg isotopic analyses and geospatial data (1,088 ± 379 Gg).[38]

RESOURCE AVAILABILITY

Lead contact

Further information and requests for resources and reagents should be directed to and will be fulfilled by the lead contact, Yanxu Zhang (yzhang127@tulane.edu).

Materials availability

This study did not generate new unique materials.

Data and code availability

The source code of the CESM2 model is available at https://github.com/ESCOMP/CESM/tree/release-cesm2.1.3. The satellite-based GFED4s fire product is available at https://www.geo.vu.nl/~gwerf/GFED/GFED4. The core code of the coupled Hg model is available at the research group website: https://www.ebmg.online/mercury.

ACKNOWLEDGMENTS

We thank Aijun Ding for helpful discussions and suggestions. This work was supported by the National Natural Science Foundation of China (grant no. 42394094 to Z.S.), the Fundamental Research Funds for the Central Universities, China (020714380216 to Z.S.), and the Postgraduate Research & Practice Innovation Program of Jiangsu Province, China (KYCX24_0207 to P.Z.).

AUTHOR CONTRIBUTIONS

Conceptualization, P.Z. and Y.Z.; methodology, P.Z., T.Y., and Y.Z.; investigation, P.Z., T.Y., Y.Z., and Z.S.; visualization, P.Z. and Y.Z.; funding acquisition, Z.S. and P.Z.; project administration, Y.Z.; supervision, Y.Z.; writing – original draft, P.Z. and Y.Z.; writing – review & editing, P.Z., Y.Z., T.Y., Z.S., D.P., M.M., Y.W., S.H., L.H., F.L., X.H., and M.W.

DECLARATION OF INTERESTS

The authors declare no competing interests.

SUPPLEMENTAL INFORMATION

Supplemental information can be found online at https://doi.org/10.1016/j.oneear.2025.101566.

Received: March 26, 2025
Revised: September 14, 2025
Accepted: December 11, 2025

REFERENCES

1. Jones, M.W., Abatzoglou, J.T., Veraverbeke, S., Andela, N., Lasslop, G., Forkel, M., Smith, A.J.P., Burton, C., Betts, R.A., van der Werf, G.R., et al. (2022). Global and Regional Trends and Drivers of Fire Under Climate Change. Rev. Geophys. *60*, e2020RG000726. https://doi.org/10.1029/2020rg000726.
2. Cunningham, C.X., Williamson, G.J., and Bowman, D.M.J.S. (2024). Increasing frequency and intensity of the most extreme wildfires on Earth. Nat. Ecol. Evol. *8*, 1420–1425. https://doi.org/10.1038/s41559-024-02452-2.
3. Wentworth, G.R., Aklilu, Y.-A., Landis, M.S., and Hsu, Y.-M. (2018). Impacts of a large boreal wildfire on ground level atmospheric concentrations of PAHs, VOCs and ozone. Atmos. Environ. *178*, 19–30. https://doi.org/10.1016/j.atmosenv.2018.01.013.
4. Rice, R.B., Boaggio, K., Olson, N.E., Foley, K.M., Weaver, C.P., Sacks, J.D., McDow, S.R., Holder, A.L., and LeDuc, S.D. (2023). Wildfires Increase Concentrations of Hazardous Air Pollutants in Downwind Communities. Environ. Sci. Technol. *57*, 21235–21248. https://doi.org/10.1021/acs.est.3c04153.
5. Friedli, H.R., Radke, L.F., and Lu, J.Y. (2001). Mercury in smoke from biomass fires. Geophys. Res. Lett. *28*, 3223–3226. https://doi.org/10.1029/2000gl012704.
6. Sigler, J.M., Lee, X., and Munger, W. (2003). Emission and Long-Range Transport of Gaseous Mercury from a Large-Scale Canadian Boreal Forest Fire. Environ. Sci. Technol. *37*, 4343–4347. https://doi.org/10.1021/es026401r.
7. Mergler, D., Anderson, H.A., Chan, L.H.M., Mahaffey, K.R., Murray, M., Sakamoto, M., and Stern, A.H.; Panel on Health Risks and Toxicological Effects of Methylmercury (2007). Methylmercury Exposure and Health Effects in Humans: A Worldwide Concern. Ambio *36*, 3–11. https://doi.org/10.1579/0044-7447(2007)36[3:Meahei]2.0.Co;2.
8. Zhang, H., Feng, X., Larssen, T., Qiu, G., and Vogt, R.D. (2010). Inland China, Rice, Rather than Fish, Is the Major Pathway for Methylmercury Exposure. Environ. Health Perspect. *118*, 1183–1188. https://doi.org/10.1289/ehp.1001915.
9. Li, H.-H., Tsui, M.T.-K., Ku, P., Chen, H., Yin, Z., Dahlgren, R.A., Parikh, S.J., Wei, J., Hoang, T.C., Chow, A.T., et al. (2022). Impacts of Forest Fire Ash on Aquatic Mercury Cycling. Environ. Sci. Technol. *56*, 11835–11844. https://doi.org/10.1021/acs.est.2c01591.
10. Baldwin, A.K., Willacker, J.J., Johnson, B.L., Janssen, S.E., and Eagles-Smith, C.A. (2024). Wildfires Influence Mercury Transport, Methylation, and Bioaccumulation in Headwater Streams of the Pacific Northwest. Environ. Sci. Technol. *58*, 14396–14409. https://doi.org/10.1021/acs.est.4c00789.
11. Brunke, E.G., Labuschagne, C., and Slemr, F. (2001). Gaseous mercury emissions from a fire in the Cape Peninsula, South Africa, during January 2000. Geophys. Res. Lett. *28*, 1483–1486. https://doi.org/10.1029/2000gl012193.
12. Weiss-Penzias, P., Jaffe, D., Swartzendruber, P., Hafner, W., Chand, D., and Prestbo, E. (2007). Quantifying Asian and biomass burning sources of mercury using the Hg/CO ratio in pollution plumes observed at the Mount Bachelor observatory. Atmos. Environ. *41*, 4366–4379. https://doi.org/10.1016/j.atmosenv.2007.01.058.
13. Friedli, H.R., Radke, L.F., Prescott, R., Hobbs, P.V., and Sinha, P. (2003). Mercury emissions from the August 2001 wildfires in Washington State and an agricultural waste fire in Oregon and atmospheric mercury budget estimates. Glob. Biogeochem. Cycles *17*. https://doi.org/10.1029/2002gb001972.
14. Friedli, H.R., Radke, L.F., Lu, J.Y., Banic, C.M., Leaitch, W.R., and MacPherson, J.I. (2003). Mercury emissions from burning of biomass from temperate North American forests: laboratory and airborne measurements. Atmos. Environ. *37*, 253–267. https://doi.org/10.1016/s1352-2310(02)00819-1.
15. Ebinghaus, R., Slemr, F., Brenninkmeijer, C.A.M., van Velthoven, P., Zahn, A., Hermann, M., O'Sullivan, D.A., and Oram, D.E. (2007). Emissions of gaseous mercury from biomass burning in South America in 2005 observed during CARIBIC flights. Geophys. Res. Lett. *34*. https://doi.org/10.1029/2006gl028866.
16. Biswas, A., Blum, J.D., Klaue, B., and Keeler, G.J. (2007). Release of mercury from Rocky Mountain forest fires. Glob. Biogeochem. Cycles *21*. https://doi.org/10.1029/2006gb002696.
17. Melendez-Perez, J.J., Fostier, A.H., Carvalho, J.A., Windmöller, C.C., Santos, J.C., and Carpi, A. (2014). Soil and biomass mercury emissions during a prescribed fire in the Amazonian rain forest. Atmos. Environ. *96*, 415–422. https://doi.org/10.1016/j.atmosenv.2014.06.032.
18. Andreae, M.O. (2019). Emission of trace gases and aerosols from biomass burning – an updated assessment. Atmos. Chem. Phys. *19*, 8523–8546. https://doi.org/10.5194/acp-19-8523-2019.
19. McLagan, D.S., Stupple, G.W., Darlington, A., Hayden, K., and Steffen, A. (2021). Where there is smoke there is mercury: Assessing boreal forest fire mercury emissions using aircraft and highlighting uncertainties associated with upscaling emissions estimates. Atmos. Chem. Phys. *21*, 5635–5653. https://doi.org/10.5194/acp-21-5635-2021.
20. Turetsky, M.R., Harden, J.W., Friedli, H.R., Flannigan, M., Payne, N., Crock, J., and Radke, L. (2006). Wildfires threaten mercury stocks in northern soils. Geophys. Res. Lett. *33*. https://doi.org/10.1029/2005gl025595.
21. Kumar, A., Wu, S., Huang, Y., Liao, H., and Kaplan, J.O. (2018). Mercury from wildfires: Global emission inventories and sensitivity to 2000–2050 global change. Atmos. Environ. *173*, 6–15. https://doi.org/10.1016/j.atmosenv.2017.10.061.

22. Friedli, H.R., Arellano, A.F., Cinnirella, S., and Pirrone, N. (2009). Initial Estimates of Mercury Emissions to the Atmosphere from Global Biomass Burning. Environ. Sci. Technol. *43*, 3507–3513. https://doi.org/10.1021/es802703g.

23. Shi, Y., Zhao, A., Matsunaga, T., Yamaguchi, Y., Zang, S., Li, Z., Yu, T., and Gu, X. (2019). High-resolution inventory of mercury emissions from biomass burning in tropical continents during 2001–2017. Sci. Total Environ. *653*, 638–648. https://doi.org/10.1016/j.scitotenv.2018.10.420.

24. Bishop, K., Shanley, J.B., Riscassi, A., de Wit, H.A., Eklöf, K., Meng, B., Mitchell, C., Osterwalder, S., Schuster, P.F., Webster, J., and Zhu, W. (2020). Recent advances in understanding and measurement of mercury in the environment: Terrestrial Hg cycling. Sci. Total Environ. *721*, 137647. https://doi.org/10.1016/j.scitotenv.2020.137647.

25. Zhang, P., and Zhang, Y. (2022). Earth system modeling of mercury using CESM2 – Part 1: Atmospheric model CAM6-Chem/Hg v1.0. Geosci. Model Dev. (GMD) *15*, 3587–3601. https://doi.org/10.5194/gmd-15-3587-2022.

26. Yuan, T., Zhang, P., Song, Z., Huang, S., Wang, X., and Zhang, Y. (2023). Buffering effect of global vegetation on the air-land exchange of mercury: Insights from a novel terrestrial mercury model based on CESM2-CLM5. Environ. Int. *174*, 107904. https://doi.org/10.1016/j.envint.2023.107904.

27. Danabasoglu, G., Lamarque, J.F., Bacmeister, J., Bailey, D.A., DuVivier, A.K., Edwards, J., Emmons, L.K., Fasullo, J., Garcia, R., Gettelman, A., et al. (2020). The Community Earth System Model Version 2 (CESM2). J. Adv. Model. Earth Syst. *12*, e2019MS001916. https://doi.org/10.1029/2019ms001916.

28. Li, F., Levis, S., and Ward, D.S. (2013). Quantifying the role of fire in the Earth system – Part 1: Improved global fire modeling in the Community Earth System Model (CESM1). Biogeosciences *10*, 2293–2314. https://doi.org/10.5194/bg-10-2293-2013.

29. van der Werf, G.R., Randerson, J.T., Giglio, L., van Leeuwen, T.T., Chen, Y., Rogers, B.M., Mu, M., van Marle, M.J.E., Morton, D.C., Collatz, G.J., et al. (2017). Global fire emissions estimates during 1997–2016. Earth Syst. Sci. Data *9*, 697–720. https://doi.org/10.5194/essd-9-697-2017.

30. Li, F., Zeng, X.D., and Levis, S. (2012). A process-based fire parameterization of intermediate complexity in a Dynamic Global Vegetation Model. Biogeosciences *9*, 2761–2780. https://doi.org/10.5194/bg-9-2761-2012.

31. Gworek, B., Dmuchowski, W., and Baczewska-Dąbrowska, A.H. (2020). Mercury in the terrestrial environment: a review. Environ. Sci. Eur. *32*, 128. https://doi.org/10.1186/s12302-020-00401-x.

32. Howard, D., Macsween, K., Edwards, G.C., Desservettaz, M., Guérette, E.-A., Paton-Walsh, C., Surawski, N.C., Sullivan, A.L., Weston, C., Volkova, L., et al. (2019). Investigation of mercury emissions from burning of Australian eucalypt forest surface fuels using a combustion wind tunnel and field observations. Atmos. Environ. *202*, 17–27. https://doi.org/10.1016/j.atmosenv.2018.12.015.

33. Fisher, J.A., and Nelson, P.F. (2020). Atmospheric mercury in Australia: Recent findings and future research needs. Elem. Sci. Anth. *8*, 070. https://doi.org/10.1525/elementa.2020.070.

34. Jain, P., Castellanos-Acuna, D., Coogan, S.C.P., Abatzoglou, J.T., and Flannigan, M.D. (2021). Observed increases in extreme fire weather driven by atmospheric humidity and temperature. Nat. Clim. Chang. *12*, 63–70. https://doi.org/10.1038/s41558-021-01224-1.

35. Su, H., Yu, Y., Guo, W., and Mao, J. (2025). Convective potential and fuel availability complement near-surface weather in regulating global wildfire activity. Sci. Adv. *11*, eadp7765. https://doi.org/10.1126/sciadv.adp7765.

36. Zheng, B., Ciais, P., Chevallier, F., Chuvieco, E., Chen, Y., and Yang, H. (2021). Increasing forest fire emissions despite the decline in global burned area. Sci. Adv. *7*, eabh2646. https://doi.org/10.1126/sciadv.abh2646.

37. Xu, J., Morris, P.J., Liu, J., and Holden, J. (2018). PEATMAP: Refining estimates of global peatland distribution based on a meta-analysis. Catena *160*, 134–140. https://doi.org/10.1016/j.catena.2017.09.010.

38. Wang, X., Yuan, W., Lin, C.J., Zhang, L., Zhang, H., and Feng, X. (2019). Climate and Vegetation As Primary Drivers for Global Mercury Storage in Surface Soil. Environ. Sci. Technol. *53*, 10665–10675. https://doi.org/10.1021/acs.est.9b02386.

39. Köchy, M., Hiederer, R., and Freibauer, A. (2015). Global distribution of soil organic carbon – Part 1: Masses and frequency distributions of SOC stocks for the tropics, permafrost regions, wetlands, and the world. Soil *1*, 351–365. https://doi.org/10.5194/soil-1-351-2015.

40. Page, S.E., Siegert, F., Rieley, J.O., Boehm, H.-D.V., Jaya, A., and Limin, S. (2002). The amount of carbon released from peat and forest fires in Indonesia during 1997. Nature *420*, 61–65. https://doi.org/10.1038/nature01131.

41. Senande-Rivera, M., Insua-Costa, D., and Miguez-Macho, G. (2022). Spatial and temporal expansion of global wildland fire activity in response to climate change. Nat. Commun. *13*, 1208. https://doi.org/10.1038/s41467-022-28835-2.

42. Outridge, P.M., Mason, R.P., Wang, F., Guerrero, S., and Heimbürger-Boavida, L.E. (2018). Updated Global and Oceanic Mercury Budgets for the United Nations Global Mercury Assessment 2018. Environ. Sci. Technol. *52*, 11466–11477. https://doi.org/10.1021/acs.est.8b01246.

43. Harris, R.M.B., Remenyi, T.A., Williamson, G.J., Bindoff, N.L., and Bowman, D.M.J.S. (2016). Climate–vegetation–fire interactions and feedbacks: trivial detail or major barrier to projecting the future of the Earth system? WIREs Clim. Change *7*, 910–931. https://doi.org/10.1002/wcc.428.

44. Jones, M.W., Kelley, D.I., Burton, C.A., Di Giuseppe, F., Barbosa, M.L.F., Brambleby, E., Hartley, A.J., Lombardi, A., Mataveli, G., McNorton, J.R., et al. (2024). State of Wildfires 2023–2024. Earth Syst. Sci. Data *16*, 3601–3685. https://doi.org/10.5194/essd-16-3601-2024.

45. Wu, C., Venevsky, S., Sitch, S., Mercado, L.M., Huntingford, C., and Staver, A.C. (2021). Historical and future global burned area with changing climate and human demography. One Earth *4*, 517–530. https://doi.org/10.1016/j.oneear.2021.03.002.

46. Zhang, G., Wang, M., Yang, B., and Liu, K. (2024). Current and Future Patterns of Global Wildfire Based on Deep Neural Networks. Earths Future *12*, e2023EF004088. https://doi.org/10.1029/2023ef004088.

47. Aguilera, R., Corringham, T., Gershunov, A., and Benmarhnia, T. (2021). Wildfire smoke impacts respiratory health more than fine particles from other sources: observational evidence from Southern California. Nat. Commun. *12*, 1493. https://doi.org/10.1038/s41467-021-21708-0.

48. Xu, R., Ye, T., Yue, X., Yang, Z., Yu, W., Zhang, Y., Bell, M.L., Morawska, L., Yu, P., Zhang, Y., et al. (2023). Global population exposure to landscape fire air pollution from 2000 to 2019. Nature *621*, 521–529. https://doi.org/10.1038/s41586-023-06398-6.

49. Silver, B., Arnold, S.R., Reddington, C.L., Emmons, L.K., and Conibear, L. (2024). Large transboundary health impact of Arctic wildfire smoke. Commun. Earth Environ. *5*, 199. https://doi.org/10.1038/s43247-024-01361-3.

50. Li, F., and Lawrence, D.M. (2017). Role of Fire in the Global Land Water Budget during the Twentieth Century due to Changing Ecosystems. J. Clim. *30*, 1893–1908. https://doi.org/10.1175/jcli-d-16-0460.1.

51. Tang, W., Tilmes, S., Lawrence, D.M., Li, F., He, C., Emmons, L.K., Buchholz, R.R., and Xia, L. (2023). Impact of solar geoengineering on wildfires in the 21st century in CESM2/WACCM6. Atmos. Chem. Phys. *23*, 5467–5486. https://doi.org/10.5194/acp-23-5467-2023.

52. Allen, R.J., Samset, B.H., Wilcox, L.J., and Fisher, R.A. (2024). Are Northern Hemisphere boreal forest fires more sensitive to future aerosol mitigation than to greenhouse gas–driven warming? Sci. Adv. *10*, eadl4007. https://doi.org/10.1126/sciadv.adl4007.

53. Chen, Y., Hall, J., van Wees, D., Andela, N., Hantson, S., Giglio, L., van der Werf, G.R., Morton, D.C., and Randerson, J.T. (2023). Multi-decadal trends and variability in burned area from the fifth version of the Global Fire Emissions Database (GFED5). Earth Syst. Sci. Data *15*, 5227–5259. https://doi.org/10.5194/essd-15-5227-2023.

54. Pan, X., Ichoku, C., Chin, M., Bian, H., Darmenov, A., Colarco, P., Ellison, L., Kucsera, T., da Silva, A., Wang, J., et al. (2020). Six global biomass burning emission datasets: intercomparison and application in one global

aerosol model. Atmos. Chem. Phys. *20*, 969–994. https://doi.org/10.5194/acp-20-969-2020.

55. Jones, M.W., Santín, C., van der Werf, G.R., and Doerr, S.H. (2019). Global fire emissions buffered by the production of pyrogenic carbon. Nat. Geosci. *12*, 742–747. https://doi.org/10.1038/s41561-019-0403-x.
56. Yuan, T., Huang, S., Zhang, P., Song, Z., Ge, J., Miao, X., Wang, Y., Pang, Q., Peng, D., Wu, P., et al. (2024). Potential decoupling of CO2 and Hg uptake process by global vegetation in the 21st century. Nat. Commun. *15*, 4490. https://doi.org/10.1038/s41467-024-48849-2.
57. Feinberg, A., Dlamini, T., Jiskra, M., Shah, V., and Selin, N.E. (2022). Evaluating atmospheric mercury (Hg) uptake by vegetation in a chemistry-transport model. Environ. Sci. Process. Impacts *24*, 1303–1318. https://doi.org/10.1039/d2em00032f.
58. Blum, J.D., and Johnson, M.W. (2017). Recent Developments in Mercury Stable Isotope Analysis. Rev. Mineral. Geochem. *82*, 733–757. https://doi.org/10.2138/rmg.2017.82.17.
59. Obrist, D., Roy, E.M., Harrison, J.L., Kwong, C.F., Munger, J.W., Moosmüller, H., Romero, C.D., Sun, S., Zhou, J., and Commane, R. (2021). Previously unaccounted atmospheric mercury deposition in a midlatitude deciduous forest. Proc. Natl. Acad. Sci. USA *118*, e2105477118. https://doi.org/10.1073/pnas.2105477118.
60. Wang, X., Yuan, W., Lin, C.-J., and Feng, X. (2021). Mercury cycling and isotopic fractionation in global forests. Crit. Rev. Environ. Sci. Technol. *52*, 3763–3786. https://doi.org/10.1080/10643389.2021.1961505.
61. Zhou, J., Obrist, D., Dastoor, A., Jiskra, M., and Ryjkov, A. (2021). Vegetation uptake of mercury and impacts on global cycling. Nat. Rev. Earth Environ. *2*, 269–284. https://doi.org/10.1038/s43017-021-00146-y.
62. Wang, X., Bao, Z., Lin, C.-J., Yuan, W., and Feng, X. (2016). Assessment of Global Mercury Deposition through Litterfall. Environ. Sci. Technol. *50*, 8548–8557. https://doi.org/10.1021/acs.est.5b06351.
63. Wright, L.P., Zhang, L., and Marsik, F.J. (2016). Overview of mercury dry deposition, litterfall, and throughfall studies. Atmos. Chem. Phys. *16*, 13399–13416. https://doi.org/10.5194/acp-16-13399-2016.
64. Zhou, J., and Obrist, D. (2021). Global Mercury Assimilation by Vegetation. Environ. Sci. Technol. *55*, 14245–14257. https://doi.org/10.1021/acs.est.1c03530.
65. Lawrence, D.M., Fisher, R.A., Koven, C.D., Oleson, K.W., Swenson, S.C., Bonan, G., Collier, N., Ghimire, B., van Kampenhout, L., Kennedy, D., et al. (2019). The Community Land Model Version 5: Description of New Features, Benchmarking, and Impact of Forcing Uncertainty. J. Adv. Model. Earth Syst. *11*, 4245–4287. https://doi.org/10.1029/2018ms001583.
66. Si, L., and Ariya, P. (2018). Recent Advances in Atmospheric Chemistry of Mercury. Atmosphere *9*, 76. https://doi.org/10.3390/atmos9020076.
67. Shah, V., Jacob, D.J., Thackray, C.P., Wang, X., Sunderland, E.M., Dibble, T.S., Saiz-Lopez, A., Černušák, I., Kellö, V., Castro, P.J., et al. (2021). Improved Mechanistic Model of the Atmospheric Redox Chemistry of Mercury. Environ. Sci. Technol. *55*, 14445–14456. https://doi.org/10.1021/acs.est.1c03160.
68. Lamarque, J.F., Emmons, L.K., Hess, P.G., Kinnison, D.E., Tilmes, S., Vitt, F., Heald, C.L., Holland, E.A., Lauritzen, P.H., Neu, J., et al. (2012). CAM-chem: description and evaluation of interactive atmospheric chemistry in the Community Earth System Model. Geosci. Model Dev. (GMD) *5*, 369–411. https://doi.org/10.5194/gmd-5-369-2012.
69. Emmons, L.K., Schwantes, R.H., Orlando, J.J., Tyndall, G., Kinnison, D., Lamarque, J.F., Marsh, D., Mills, M.J., Tilmes, S., Bardeen, C., et al. (2020). The Chemistry Mechanism in the Community Earth System Model Version 2 (CESM2). J. Adv. Model. Earth Syst. *12*, e2019MS001882. https://doi.org/10.1029/2019ms001882.
70. Liu, X., Ma, P.L., Wang, H., Tilmes, S., Singh, B., Easter, R.C., Ghan, S.J., and Rasch, P.J. (2016). Description and evaluation of a new four-mode version of the Modal Aerosol Module (MAM4) within version 5.3 of the Community Atmosphere Model. Geosci. Model Dev. (GMD) *9*, 505–522. https://doi.org/10.5194/gmd-9-505-2016.
71. Yuan, W., Sommar, J., Lin, C.-J., Wang, X., Li, K., Liu, Y., Zhang, H., Lu, Z., Wu, C., and Feng, X. (2019). Stable Isotope Evidence Shows Re-emission of Elemental Mercury Vapor Occurring after Reductive Loss from Foliage. Environ. Sci. Technol. *53*, 651–660. https://doi.org/10.1021/acs.est.8b04865.
72. Liu, Y., Liu, G., Wang, Z., Guo, Y., Yin, Y., Zhang, X., Cai, Y., and Jiang, G. (2021). Understanding foliar accumulation of atmospheric Hg in terrestrial vegetation: Progress and challenges. Crit. Rev. Environ. Sci. Technol. *52*, 4331–4352. https://doi.org/10.1080/10643389.2021.1989235.
73. Hintelmann, H., Harris, R., Heyes, A., Hurley, J.P., Kelly, C.A., Krabbenhoft, D.P., Lindberg, S., Rudd, J.W.M., Scott, K.J., and St Louis, V.L. (2002). Reactivity and mobility of new and old mercury deposition in a boreal forest ecosystem during the first year of the METAALICUS study. Mercury Experiment To Assess Atmospheric Loading In Canada and the US. Environ. Sci. Technol. *36*, 5034–5040. https://doi.org/10.1021/es025572t.
74. Zhang, H., Nizzetto, L., Feng, X., Borgå, K., Sommar, J., Fu, X., Zhang, H., Zhang, G., and Larssen, T. (2019). Assessing Air–Surface Exchange and Fate of Mercury in a Subtropical Forest Using a Novel Passive Exchange-Meter Device. Environ. Sci. Technol. *53*, 4869–4879. https://doi.org/10.1021/acs.est.8b06343.
75. Obrist, D., Faïn, X., and Berger, C. (2010). Gaseous elemental mercury emissions and CO2 respiration rates in terrestrial soils under controlled aerobic and anaerobic laboratory conditions. Sci. Total Environ. *408*, 1691–1700. https://doi.org/10.1016/j.scitotenv.2009.12.008.
76. Kohlenberg, A.J., Turetsky, M.R., Thompson, D.K., Branfireun, B.A., and Mitchell, C.P.J. (2018). Controls on boreal peat combustion and resulting emissions of carbon and mercury. Environ. Res. Lett. *13*, 035005. https://doi.org/10.1088/1748-9326/aa9ea8.
77. Johnston, F.H., Henderson, S.B., Chen, Y., Randerson, J.T., Marlier, M., DeFries, R.S., Kinney, P., Bowman, D.M.J.S., and Brauer, M. (2012). Estimated Global Mortality Attributable to Smoke from Landscape Fires. Environ. Health Perspect. *120*, 695–701. https://doi.org/10.1289/ehp.1104422.
78. Ward, D.S., Kloster, S., Mahowald, N.M., Rogers, B.M., Randerson, J.T., and Hess, P.G. (2012). The changing radiative forcing of fires: global model estimates for past, present and future. Atmos. Chem. Phys. *12*, 10857–10886. https://doi.org/10.5194/acp-12-10857-2012.
79. Sprovieri, F., Pirrone, N., Bencardino, M., D'Amore, F., Carbone, F., Cinnirella, S., Mannarino, V., Landis, M., Ebinghaus, R., Weigelt, A., et al. (2016). Atmospheric mercury concentrations observed at ground-based monitoring sites globally distributed in the framework of the GMOS network. Atmos. Chem. Phys. *16*, 11915–11935. https://doi.org/10.5194/acp-16-11915-2016.
80. Jiskra, M., Sonke, J.E., Obrist, D., Bieser, J., Ebinghaus, R., Myhre, C.L., Pfaffhuber, K.A., Wängberg, I., Kyllönen, K., Worthy, D., et al. (2018). A vegetation control on seasonal variations in global atmospheric mercury concentrations. Nat. Geosci. *11*, 244–250. https://doi.org/10.1038/s41561-018-0078-8.
81. Horowitz, H.M., Jacob, D.J., Zhang, Y., Dibble, T.S., Slemr, F., Amos, H.M., Schmidt, J.A., Corbitt, E.S., Marais, E.A., and Sunderland, E.M. (2017). A new mechanism for atmospheric mercury redox chemistry: implications for the global mercury budget. Atmos. Chem. Phys. *17*, 6353–6371. https://doi.org/10.5194/acp-17-6353-2017.
82. Holmes, C.D., Jacob, D.J., Corbitt, E.S., Mao, J., Yang, X., Talbot, R., and Slemr, F. (2010). Global atmospheric model for mercury including oxidation by bromine atoms. Atmos. Chem. Phys. *10*, 12037–12057. https://doi.org/10.5194/acp-10-12037-2010.